Anonymous Referee #1

General Comments

This paper combines the use of an optical model and field observations to look at the potential impact of boat wakes on the optical properties of the water column near seagrass beds. The optical measurements and modeling are fairly routine, but the combination with wave height data to examine the impact of boat wakes is unique and important. The paper is easy to read.

We appreciate the support of the paper. We do believe that the extended, continuous measurements of light attenuation and light attenuating substances are relatively unique, especially in a back-barrier estuary.

Specific Comments

The calculation of the areal coverage of seagrass at the end of section 2.1 is unnecessary and should be considered for removing.

We added those details so that the influence of vegetation on the wave characteristics and resuspension could be assessed. We believe that the relative density of vegetation, while similar in this case, should be noted to account for any differences in wave height or resuspension response. Specifically, if the densities were markedly different between the sites, the inferences made in Figure 9 about sediment availability would be less robust as changes in density could account for changes in turbidity at a given shear stress.

Section 2.2. Because of the similarities in spectral shape of many of the model components is appears like you are pushing all the error into the CDOM component. Nothing necessary to change, but something to stay aware of.

After the submission of this paper we quantified substantial changes in CDOM/fDOM/composition in Barnegat Bay (as well as two other estuaries) that suggest a highly variable relationship between fDOM and CDOM, that is related to isotopic composition (highlighting the influence of carbon source on optical properties). We have added this statement on line 6, pg. 11:

> ***The variability in the fDOM vs. salinity relationship supports the possibility that the source and optical properties of colored organic matter varies spatially in Barnegat Bay; Oestreich et al. (2014) demonstrated large spatial variability in CDOM absorbance potential per unit fluorescence, as a function of source.***

Section 4.1. It would be nice to add a discussion on why the model flattens out and observations don't in Figure 8.

We agree. In that range of the comparison (i.e. modeled Kd < 1.6), the magnitude and variability in turbidity, chl-a, fDOM were low, but the PAR measurements indicated some variability in Kd. We surmise this could be due to changes in either particle characteristics or other effects that would be more obvious at low attenuation, such as surface wave effects. It is also possible that the model parameterization for the three substances fails at the low end (because the parameters are not static). We chose to optimize the relationship for high KD,

but one can imagine selecting parameters to optimize for agreement at the low end. We have added this text on lines 28-4, pg. 11-12:

> ***At the lower end of the comparison between observed and modeled Kd (i.e. modeled Kd <1.6), we find reduced sensitivity of the model to changes in observed turbidity, chl-a, and fDOM. This could be due to changes in either particle characteristics or other effects that would be more obvious at low attenuation, such as interference from surface waves. It is also possible that the model parameterization for the three attenuating substances fails at the low end because the parameters (Table 4) are not static. We chose to optimize the relationship for high KD, but could have alternatively selected parameters to optimize for agreement at the low end.***

Section 4.1 Keep in mind that the shape of the scattering function is dependent on both the index of refraction and the size of the particles. This makes the general statement about the scattering by organic and inorganic particles on page 12195 a little weak.

We agree, and have modified to reflect the source material from Gallegos et al. (2011). The statement on line 16, pg. 11 now reads:

> ***While scattering by organic particles is strongly in the forward direction (smaller value of bb(part)), mineral particles, having larger refraction indices, scatter a greater fraction of light in the backward direction (larger bb(part)). The dependency of backscattering on particle size results in smaller modifications of bb(part) than the refraction index differences between organic and mineral particles (Gallegos et al., 2011). Thus a larger backscattering ratio was expected in the areas with higher turbidity (site LEI).***

Anonymous Referee #2

General Comments: As indicated by the title, this manuscript describes the use of combined high-frequency, in situ optical and wave gauge measurements with an optical model to investigate the impact of boat wakes on the diffuse attenuation measured over wavelengths representing the photosynthetically active region (PAR) of the water column near seagrass beds. Overall the manuscript is well organized and the writing is clear and concise. The strength of the manuscript lies in the main message conveyed by the authors – high-frequency measurements are necessary to expose the scale of the variability in diffuse attenuation measurements, critical in understanding seagrass community restoration success and estimating the recovery of estuaries from eutrophication.

We appreciate the reviewer's recognition of our goals in the manuscript.

The only disparaging comment I have about the manuscript is that the reader may be confused by discussions of backscatter, scatter and backscatter ratio measurements, which need to be better explained in the manuscript. I am not certain whether backscatter related terms are inverted from equation 2 or were directly measured. Seems as least backscatter may have been measured in situ, but not inverted from the data?

We have clarified these terms wherever incorrectly noted (see below). The most important point is that our instruments are calibrated to turbidity standards, and are not reporting backscatter. Most of our use of those terms come directly from the light modeling paper of Gallegos et al. (2011), and we have one instance of erroneous usage (see below).

Specific Comments:

1. Use of FDOM and spectral slope of CDOM interchanges in equation 2

a. Use of a fixed spectral slope without knowledge of at least some knowledge of CDOM spectral absorption in at least a few discrete samples from the study area.

We conducted a sensitivity analysis on all fixed parameters and found little effect of varying spectral slope. Work conducted after submission (Oestreich et al., 2014) quantified CDOM spectral slopes in Barnegat Bay, and found approximately a 15% change in spectral slope between our sites. Using this range of spectral slopes in Eq. 2 changed K_{dPAR} less than 4%. This is because we are dealing with a narrow spectrum (400-700 nm) instead of the entire spectrum, and peak absorbance is occurring at the part of the spectrum where we are assigning the reference value (440 nm). We have noted the variability on Pg 11, lines 6-11, as:

The variability in the fDOM vs. salinity relationship supports the possibility that the source and optical properties of colored organic matter varies spatially in Barnegat Bay.; Oestreich et al. (2014) demonstrated large spatial variability in CDOM absorbance potential per unit fluorescence, as a function of source. Spectral slope within Barnegat Bay varied by approximately 15%, resulting in calculated changes to K_{dPAR} of less than 4%.

b. Use of in situ FDOM with respect to non-linearity effects due to particle interference or concentration related quenching effects. Some researchers have seen non-linearity effects on FDOM due to particles at turbidities as low as 20 NTU.

We agree that the interference from turbidity has been noted, however we did not observe a strong relationship (see figure below). For example, at site LEI we have daily turbidity changes exceeding 70 NTU, with a concurrent decrease in fDOM of less than 2 QSU. Overall, there is a low correlation between the two signals (r^2=0.08). We have noted this in the text on Pg 8, lines 6-8 as:

> **Prior work has demonstrated the interference of turbidity with fDOM measurement (Downing et al., 2012); we found low correlation (r2=0.08) between fDOM and turbidity at this site.**

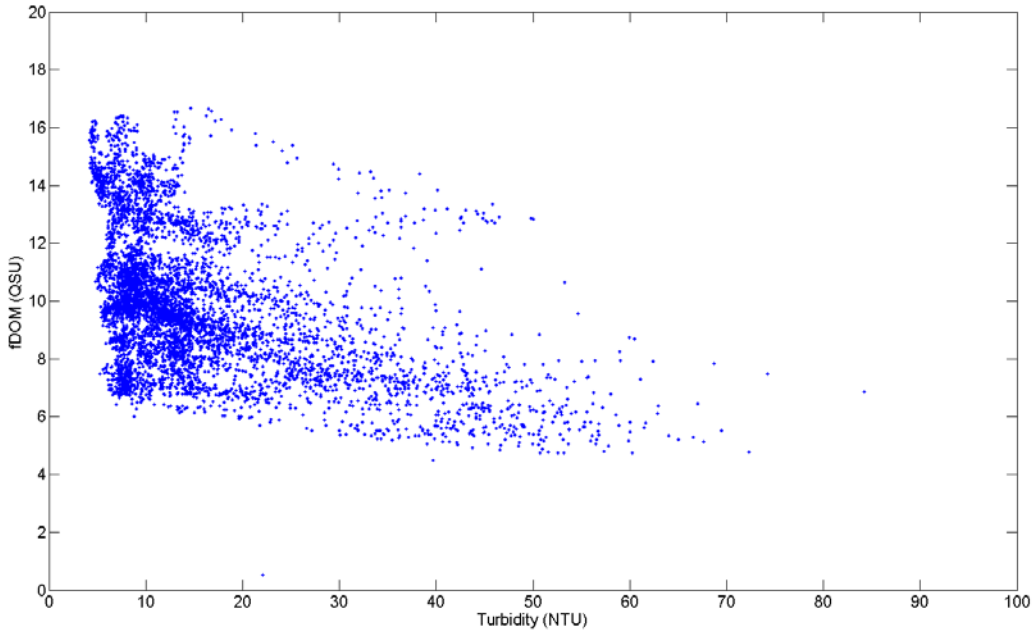

2. Use of backscatter ratio in the paper. Instruments used in the study are capable of obtaining backscatter, but not reported?

We are not capable of measuring backscattering ratio with the instruments we deployed. We have erroneously used the term "backscatter" in one location where we intended "backscatter ratio" (noted below). The instruments we are using (YSI EXO, ECO NTUSB) are all intercalibrated to formazin turbidity standards, and are inverting a voltage signal internally to turbidity.

Other comments and questions: Was the bottom PAR sensor located in the fluidized sediment? What about the optical sensing volume, particle interference and likely beam attenuation along the pathlength of the sensing volume? How was this addressed as this would certainly affect response linearity.

All instruments other than the upper PAR sensor are at approximately 0.15 meters above bottom, and the peak turbidity we measured at any point was about 100 NTU (corresponding to roughly 150 mg/L based on historic SSC calibrations). By definition, fluid mud is well over this concentration. Nonetheless, there are certainly vertical gradients in concentration that will affect our calculations (see response below). In terms of sensing volume, the PAR sensor is a light receptor that is measuring PAR as delivered through the entire water column above it.

Kd should be annotated as Kd (PAR).

This has been corrected throughout.

The calculation for Kd assumes linearity between the irradiance measurement with depth in the water column. With only two PAR sensors located at fixed depth (top and bottom) that forces linearity. The lower PAR sensor located in the fluidized sediment may not accurately represent the light field at the benthos due to particle interferences?

The $K_{d\text{PAR}}$ calculation is by definition the attenuation between the two sensors (separated by 0.3 m). There could certainly be vertical variability in $K_{d\text{PAR}}$ higher in the water column. But by using a fixed distance, we are able to compare sites with an emphasis towards the bottom 0.5 m of the water column, where seagrass and other benthic flora are established. The most important assumption we are making in our other calculations is that the constituent concentration is uniform between the two sensors. We have added text to this effect on Pg 11-12 lines 28-4 (added to discussion requested by Reviewer 1):

> ***At the lower end of the comparison between observed and modeled K_{dPAR} (i.e. modeled K_{dPAR} <1.6), we find reduced sensitivity of the model to changes in observed turbidity, chl-a, and fDOM. This could be due to changes in either particle characteristics or other effects that would be more obvious at low attenuation, such as interference from surface waves. It is also possible that the model parameterization***

for the three attenuating substances fails at the low end because the parameters (Table 4) are not static. We are also assuming that constituent concentrations are uniform between the two PAR sensors; changes in vertical gradients between quiescent and energetic periods could also alter the agreement. We chose to optimize the relationship for high K_{dPAR}, but could have alternatively selected parameters to optimize for agreement at the low end.

"Backscattering caused by water molecules was the largest bb effect ": : : This is confusing to me. Is the intention to show the reader that as a modelling exercise, bb of water impacts the model more as a variable or actual measured bb?

This is an error. The backscattering ratio (fraction of backscatter in the backwards direction) of water is larger than the backscattering ratio of particles, but the actual backscatter from water is substantially less than particles. This has been corrected on Pg 6 lines 19-23 as:

The backscattering ratio of water was set at 0.5, while CDOM is considered nonscattering (Mobley and Stramski, 1997), and the particulate effective backscattering ratio was initially set at 0.015.

According to your methods section, a WETLabs ECO NTUSB sensor was used to measure turbidity. You do not mention that backscatter was inverted from the sensor anywhere in the manuscript. Was the sensor characterized to obtain backscatter? How did you obtain backscatter then? Ultimately how was the backscattering ratio determined, since scatter (b), was not measured either. This needs to be clarified in the manuscript. No? A time series of the backscatter would greatly add to the manuscript.

I think this comment springs from the aforementioned error ("backscattering" instead of "backscattering ratio"). We do not directly measure backscatter anywhere, our sensors are reporting turbidity and are calibrated to formazin standards. Backscattering ratios were initially set using Gallegos et al. (2011), and particulate backscattering ratio was modified to account for site LEI's higher turbidity (and potentially higher fraction of mineral composition). This is noted on Pg 11 lines 16-21:

Additionally, variability in turbidity and organic content of suspended sediment also suggests that particulate backscattering ratio may be spatially variable; suspended-sediment samples demonstrated organic content ranging from 13% at site LEI to 60% at site LVL. The backscattering ratio change from 0.015 to 0.025 at LEI_{sh} is within the range (0.0024 to 0.06, Loisel et al., 2007 and Snyder et al., 2008) provided by Gallegos et al. (2011). While scattering by organic particles is strongly in the forward direction

(smaller value of $b_{b(part)}$), mineral particles, having larger refraction indices, scatter a greater fraction of light in the backward direction (larger $b_{b(part)}$). The dependency of backscattering on particle size results in smaller modifications of $b_{b(part)}$ than the refraction index differences between organic and mineral particles (Gallegos et al., 2011). Thus a larger backscattering ratio was expected in the areas with higher turbidity (site LEI).

Physical and biogeochemical controls on light attenuation in a eutrophic, back-barrier estuary

N. K. Ganju[1], J.L. Miselis[2], and A.L. Aretxabaleta[1]

[1]{U.S. Geological Survey, Woods Hole, Massachusetts}

[2]{U.S. Geological Survey, St. Petersburg, Florida}

Correspondence to: N. K. Ganju (nganju@usgs.gov)

Abstract

Light attenuation is a critical parameter governing the ecological function of shallow estuaries. In these systems primary production is often dominated by benthic macroalgae and seagrass; thus light penetration to the bed is of primary importance. We quantified light attenuation in three seagrass meadows in Barnegat Bay, New Jersey, a shallow eutrophic back-barrier estuary; two of the sites were located within designated Ecologically Sensitive Areas (ESAs). We sequentially deployed instrumentation measuring photosynthetically active radiation, chlorophyll-a (chl-a) fluorescence, dissolved organic matter fluorescence (fDOM; a proxy for colored DOM absorbance), turbidity, pressure, and water velocity at 10 min intervals over three week periods at each site. At the southernmost site, where sediment availability was highest, light attenuation was highest and dominated by turbidity and to a lesser extent chl-a and CDOM. At the central site, chl-a dominated followed by turbidity and CDOM, and at the northernmost site turbidity and CDOM contributed equally to light attenuation. At a given site, the temporal variability of light attenuation exceeded the difference in median light attenuation at the three sites, indicating the need for continuous high-temporal resolution measurements. Vessel wakes, anecdotally implicated in increasing sediment resuspension, did not contribute to local resuspension within the seagrass beds, though frequent vessel wakes were observed in the channels. With regards to light attenuation and water clarity, physical and biogeochemical variables appear to outweigh any regulation of boat traffic within the ESAs.

1 Introduction

Back-barrier estuaries, especially along the Atlantic coast of the United States, are typically shallow systems colonized by benthic primary producers (Ziegler and Benner, 1998; Meyercordt et al., 1999; McGlathery et al., 2001). Prior to urbanization and agricultural influence in the watersheds, many systems were characterized by high densities of seagrass and relatively low light attenuation. Subsequent nutrient loading resulting from industrial and agricultural development has led to a gradual decline in seagrass density as eutrophication created water-column algal blooms and overgrowth of benthic algae (Burkholder et al., 2007). Both of these algal succession processes reduce light penetration to seagrass colonies. Evaluating the resiliency of remaining seagrass colonies requires understanding the relative importance of the mechanisms controlling light attenuation in the water column.

There are generally four major factors that reduce light penetration in the water column: the water itself (a function of depth), non-algal particulate material (i.e. suspended sediment), phytoplankton biomass, and colored dissolved organic matter (CDOM) (Kirk, 1994). Generally proxies are used to estimate these quantities *in-situ*: turbidity, chlorophyll-a fluorescence, and fluorescing DOM (fDOM). In estuaries, depth is governed by geomorphology and tidal elevations, therefore light attenuation caused by water is maximized in the deepest channels at high tide, and minimized over shoals at low tide. Suspended-sediment concentrations are typically controlled by supply from external sources or local resuspension from the sediment bed (Schoellhamer, 2002). Supply is a function of tidal advection (or riverine input) from a non-local repository, while local resuspension can be instigated by tidal currents or wave action (Ganju et al., 2004). Chlorophyll-a concentrations represent the abundance of phytoplankton in the water column, which is a function of nutrient loading, residence time, advection, grazing by zooplankton, and other factors (Phlips et al., 2002; Howarth and Marino, 2006; Glibert et al., 2007). Estuaries with high nutrient loading and long residence time tend to have the highest chlorophyll-a concentrations; locations within the estuary far from the nutrient source may experience elevated concentrations due to tidal advection. CDOM is typically associated with a terrestrial end member, leading to an inverse correlation between salinity and CDOM; concentrations may also be elevated in areas draining marsh plains (Downing et al., 2009) and terrestrial watersheds (Spencer et al., 2013).

Instrument limitations typically preclude high temporal resolution (~1 h) of these parameters over extended periods (i.e. spring-neap cycle). Light and other optical sensors are prone to

rapid biofouling and it is logistically difficult to occupy multiple stations within an estuary. Several studies have quantified the spatial and temporal variability of light attenuation in estuaries, though the spatial and temporal scales vary widely. Phlips et al. (1995) sampled monthly at 17 stations within Florida Bay for one year and described spatial variability in light attenuation due to variability in non-algal turbidity and phytoplankton concentrations. Christian and Sheng (2003) conducted synoptic sampling over a 3-mo period in the Indian River Lagoon and found that non-algal particulates dominated light attenuation. Both of these studies used non-autonomous light sensors and laboratory determination of chlorophyll-a and suspended sediment, thereby limiting temporal resolution. However, with a combination of high-frequency point observations and modeling, Lawson et al. (2007) investigated the influence of suspended sediment on light attenuation in a coastal lagoon and determined that infrequent point monitoring was inadequate for characterizing light dynamics for benthic flora.

The Barnegat Bay-Little Egg Harbor estuary (BBLEH) is a back-barrier estuary on the New Jersey coast (Fig. 1). BBLEH is connected to the Atlantic Ocean via three inlets and is characterized by extensive shallows and maintained navigation channels. The shallows of BBLEH are colonized by seagrass beds of *Zostera marina* and *Ruppia maritima*, depending on salinity conditions, with the salt-tolerant *Z. marina* mostly in the southern portion of the system (Kennish et al., 2013). The influence of the Toms River (and other freshwater sources) lowers salinity in the northern portion of the system, leading to a shift towards *R. maritima*. Seagrass meadows rely on adequate light conditions to maintain productivity and their presence in estuarine systems; changes in light attenuation, sediment quality, and water quality can threaten the persistence of seagrasses. In BBLEH, eutrophication due to anthropogenic nutrient loading has led to decreased water clarity, increased macroalgal proliferation, and frequent hypoxia (Kennish et al., 2007; Kennish et al., 2011). Concurrently, decreases in areal seagrass meadow coverage have been observed using a combination of remote sensing and field surveys (Lathrop et al., 2006). Within BBLEH, several Ecologically Sensitive Areas (ESAs) have been designated to lessen the effect of both vessel wakes and propeller scars. Many of the ESAs are centered on seagrass meadows, while other well-colonized areas are not within a protected zone. In this study, we aim to quantify the constituents and mechanisms governing light attenuation within seagrass meadows in BBLEH with high temporal resolution at multiple sites. We first detail the observational methods and results of the time-series analysis. We then discuss the spatiotemporal variability of light

attenuation, assign relative contributions from different constituents, address the possible role of vessel wakes and wind-waves on sediment resuspension, and discuss the role of sediment availability on spatial differences in light attenuation. Finally, we compare the differences in light and wave climate between ESAs and non-ESAs, and high-vessel-traffic areas vs. low-vessel-traffic areas.

2 Methods

2.1 Field observations

We developed a shallow-water platform designed to measure light attenuation and attenuating constituents in the bottom half of a 1 m water column. The platform consisted of an RBR D|Wave recorder, a pair of WetLabs ECO-PARSB self-wiping photosynthetically active radiation (PAR, 400-700 nm) sensors; a YSI EXO multisonde measuring temperature, salinity, turbidity, chlorophyll-a fluorescence, fluorescing dissolved organic matter (fDOM, a proxy for CDOM), pH, and depth; and a Nortek Aquadopp-HR 1 MHz current profiler. All instruments except for the upper PAR sensor were mounted at 0.15 meters above the bed (mab) on a weighted fiberglass grate approximately 1 m x 0.5 m. The lower PAR sensor was recessed inside a PVC tube protruding from the bottom of the frame, intended to penetrate into the bed. At two sites this required a water-jet apparatus to fluidize the sediment bed and facilitate penetration; turbidity plumes typically subsided within 1 h. The upper PAR sensor was mounted at 0.45 mab to provide an estimate of light attenuation K_{dPAR} over the PAR spectrum (400-700 nm), calculated as:

$$K_{dPAR} = -\frac{1}{dz}\ln(PAR_{lower}/PAR_{upper}) \quad (1)$$

where *dz* is the distance between the two PAR sensors (0.3 m in this case). Light attenuation was calculated only between the hours of 1030 and 1530, when the angle of the sun relative to the deployment location was closest to 0 degrees (for the June-September period). A second instrument package consisted of an RBR-D|Wave and a WetLabs ECO-NTUSB to measure turbidity; this package was deployed in the navigation channel closest to each site. The platform was attached to vertical structures with the sensors approximately 1.5 m below the water surface at mid-tide. All sensors sampled at intervals between 5-10 min, except for the wave recorders which sampled continuously at 6 Hz. Significant wave height and period were

calculated using zero-upcrossing statistics over 20 min windows; peak parameters were estimated with a 20 sec window. We identified vessel wakes by comparing the ratio of peak significant wave height over short time windows (20 s) with the wave height over longer time windows (20 min); this technique highlights infrequent increases in wave height that are most likely caused by passing vessels. Spectral density estimates for turbidity, chlorophyll-a, and fDOM were made using the WAFO toolbox (Brodtkorb et al., 2000).

We sequentially occupied three shoal/channel sites during the 25 June 2013 – 13 September 2013 period (Fig. 1). From south to north, Little Egg Island (LEI_{sh}) and the Route 72 bridge (LEI_{chan}) were occupied from 25 June – 15 July 2013; Tice's Shoal (TS_{sh}) and ICWW marker 28 (TS_{chan}) were occupied from 16 July – 13 August 2013; and Lavalette (LVL_{sh}) and ICWW marker 40 (LVL_{chan}) were occupied from 14 August -12 September 2013. Depths were 0.9 m at site LEI_{sh}, 0.8 m at site TS_{sh}, and 0.6 m at site LVL_{sh}. Depths at channel sites varied but instruments were maintained at a depth of 1.5 m below surface at mid-tide.

As mentioned above, portions of Barnegat Bay are designated as ESAs, and boaters are encouraged to avoid these areas to minimize damage to seagrass and benthic habitats. Nonetheless, some ESAs experience substantial recreational vessel traffic. Shoal sites were chosen to coincide with one of three archetypes: an ESA with minimal vessel traffic (site LEI_{sh}), an ESA with substantial vessel traffic (site TS_{sh}), and a non-ESA with substantial vessel traffic (site LVL_{sh}). At all three sites, we chose areas with seagrass coverage but deployed the platform on bare patches of the bed within the meadow. Bare patches were typically 10 m^2, but surrounded on all sides by vegetation. Kennish et al. (2013) documented seasonal and spatial characteristics of seagrass meadows in Barnegat Bay. We averaged values from the June-September time period, and summed biomass and areal coverage of all species. Northern locations are dominated by *Ruppia* with total dry biomass of 9 g/m^2 and 24% areal coverage, central locations are dominated by *Zostera* with total dry biomass of 14 g/m^2 and 32% areal coverage, and southern locations are entirely *Zostera* with total dry biomass of 10 g/m^2 and 26% areal coverage.

2.2 Estimation of light attenuation contributions

Preisendorfer (1976) linked K_{dPAR} with the inherent optical properties (IOPs) including absorption (a), scattering (b), and/or backscattering (b_b) coefficients. As measuring scattering accurately remains operationally difficult, Lee et al. (2005) introduced a semi-analytical

formulation based only on absorption and backscattering. Gallegos et al. (2011) adopted this approach and adapted it for spectral irradiance to take the form:

$$K_d(\lambda) = (1 + 0.005\,\theta_0)\,a(\lambda) + 4.18\left(1 - 0.52\,e^{-10.8\,a(\lambda)}\right) b_b(\lambda) \quad (2)$$

where θ_0 is the solar incidence angle in degrees, and $K_{dPAR}(\lambda)$, $a(\lambda)$ and $b_b(\lambda)$ are the spectral attenuation, absorption and backscattering at frequency λ.

In this study, we use the Gallegos et al. (2011) formulation that computes the quantities needed to form spectral attenuation in terms of suspended and dissolved constituents including the effects of water, CDOM, phytoplankton, and non-algal particulates (NAP, e.g., detritus, minerals, bacteria). We include absorption by four components: (1) absorption by water was assumed to follow the spectral characteristics of pure water; (2) CDOM absorption was taken proportional to fDOM concentration, with a negative spectral slope (Bricaud et al., 1981) set to s_g=0.0177 nm^{-1} (within the range of values measured by Gallegos et al., 2011); (3) phytoplankton absorption was proportional to chlorophyll-a concentration and with the spectrum shape normalized by the absorption peak at 675 nm (initial value for peak absorption was taken as $a_{\phi,675}$=0.0235 m^2 (mg Chl-a)$^{-1}$, within the range provided by Bricaud et al., 1995); and (4) non-algal absorption was taken as proportional to the total suspended solids (TSS) concentration with a spectral shape (Bowers and Binding, 2006) that included a baseline of c_{x1}=0.0024 m^2 g^{-1} (Biber et al., 2008), an absorption cross-section of c_{x2}=0.04 m^2 g^{-1} (Bowers and Binding, 2006), and a spectral slope of s_x=0.009 (Boss et al., 2001). The ~~B~~backscattering ratio of water ~~caused by water molecules was the largest b_b effect with a ratio of~~was set at 0.5, while CDOM is considered nonscattering (Mobley and Stramski, 1997), and the particulate effective backscattering ratio was initially set at~~much smaller (initial value set to 0.015)~~. The composition of NAP in most environments is largely unknown and rapidly changing resulting in a large variability in the relationship between TSS, absorption and backscattering. While Gallegos et al. (2011) introduced a range of values depending on the different components of the NAP pool, we chose a constant set of parameters that represented averaged conditions; ultimately the relationship between fDOM and CDOM absorbance appeared to be variable (see below). These parameters were varied to obtain the best agreement between observations and the model.

2.3 Sediment sampling methods

Bed sediment samples were collected from the estuarine floor using the mini-SEABOSS system (Valentine et al., 2000), which uses a modified Van Veen sediment grab to collect 0.1 m^2 undisturbed seafloor sample. Samples in water less than 1 m depth (adjacent to the deployment sites) were collected with a hand-held shovel. The upper 2 cm of the recovered sediment was sampled with a scoop and bagged for textural analysis. Approximately 50 g of wet sample were wet sieved through a 0.062 mm sieve to separate the coarse and fine fractions. Coarse fractions (sand and gravel) were oven-dried, weighed and dry-sieved. Fine fractions (silt and clay) were analyzed using a Coulter Counter Multisizer 3. The combination of both techniques allows for the weight percentages of grain sizes from -5 to 11 phi to be determined. The sediment classification and frequency percentages were calculated using GSSTAT software (Poppe et al., 2004), which is based on the methods of Folk (1974) and Collias et al. (1963). Most sampling locations were optimized to groundtruth boat-based acoustic backscatter data rather than to characterize the sites at which light attenuation was measured, and were therefore depth-limited. At sites LVL_{sh} and TS_{sh}, there were several samples within 2 km of the instrumentation, and a single sample adjacent to each deployment site. At site LEH_{sh}, other than the deployment-adjacent sample, the closest sediment samples were approximately 5 km away.

3 Results

3.1 Temporal variability of light attenuation, constituents, and physical forcing

We discuss the characteristics of the time-series at all shoal sites from south to north, beginning with site LEI_{sh}. Maximum tidal range was about 0.75 m during spring tides (Fig. 2), though water velocity rarely exceeded 0.20 m/s. PAR was successfully measured at the upper sensor, but the lower sensor unexpectedly failed after 5 days, which precludes the direct measurement of K_{dPAR} over the entire record. We used Eq. 2 to reconstruct K_{dPAR} for the remainder of the time period; details of the application of Eq. 2 are given at the end of this section. K_{dPAR} exceeded 7 m^{-1} during periods with high turbidity. Turbidity exceeded 50 NTU on several days, due to M_2 periodic (12.42 h) tidal advection and diurnal wind-wave resuspension (Figs. 2, 3, 4). Chl-a demonstrated a diurnal signal (Figs. 2, 4), with troughs during peak daylight (and peaks during lowest light); this is a characteristic signature of non-

photochemical quenching (NPQ) whereby chlorophyll fluorescence is reduced at high levels of irradiance (Fig. 5; Maxwell and Johnson, 2000; Lawrenz and Richardson, 2011). Given the long residence time in Barnegat Bay (Defne and Ganju, ~~in revision~~2014), it is most likely that NPQ is responsible for these changes rather than tidal advection or daily changes in phytoplankton concentration. The concentration of fDOM was relatively low and constant (Fig. 2) showing a stable relationship with salinity (Fig. 6). Prior work has demonstrated the interference of turbidity with fDOM measurement (Downing et al., 2012); we found low correlation (r^2=0.08) between fDOM and turbidity at this site. Significant wave height approached 0.1 m, peaking daily during periods of winds from the south (Fig. 3); peak wave height was 0.14 m. This led to a concurrent increase in turbidity during wave events. Wave period ranged from 1.4 to 2.4 s; peak wave periods over 4 s were observed and attributed to vessel passage due to their anomalous nature (not shown). At the channel site, wave heights were almost three times greater (not shown), but out of phase with wind speed. Wave heights in the channel peaked during times with ostensibly more vessel traffic (weekends, early afternoon). We explore the wave characteristics and their relationship to vessel passage at this site further in the Discussion section.

Formatted: Superscript

At site TS_{sh}, maximum tidal range was less than 0.40 m, and water velocity was less than 0.20 m/s with substantial subtidal variability (Fig. 2). The reduction in tide range and larger influence of subtidal processes on hydrodynamics in northern Barnegat Bay corroborates prior studies (Chant, 2001; Defne and Ganju, ~~in revision~~2014). PAR was successfully measured at both sensors during the entirety of the deployment. K_{dPAR} peaked over 3 m^{-1} during a frontal passage on 25 July 2013; strong winds from the north led to a wind-wave sediment resuspension event, and increased river runoff from the Toms River decreased salinity and raised fDOM levels. Apart from the duration of this event, turbidity was less than 20 NTU. Chl-a again demonstrated a diurnal signal (Fig. 4), with troughs during peak daylight (and peaks during lowest light); non-photochemical quenching was again suspected (Fig. 5). The concentration of fDOM was higher than site LEI_{sh}, with a peak during the event of 25 July 2013 (Fig. 2); the relationship with salinity strayed slightly from the relationship at site LEI_{sh}, suggesting a different source of fDOM (Fig. 6). Significant wave height was less than 0.1 m, peaking during periods of strongest winds (Fig. 3); peak wave height was 0.17 m. Wave period ranged from 1.4 to 3.5 s; peak wave periods over 5 s were observed regularly (not shown). At the channel site, wave heights were over 0.3 m (not shown).

The northernmost site LVL_{sh} had a tidal range of less than 0.40 m, with velocities exceeding 0.3 m/s during meteorological events (Fig. 2). PAR was successfully measured at both sensors during all but the last week of the deployment. K_{dPAR} peaked at over 3.0 m^{-1} during another frontal passage on 1 September 2013; strong winds from the south led to a wind-wave sediment resuspension event with turbidity exceeding 20 NTU. Apart from the duration of this event, turbidity was less than 20 NTU. Non-photochemical quenching was again observed in the chl-a time-series (Fig. 5). The concentration of fDOM was higher than site TS_{sh}, but relatively constant (Fig. 2). The relationship with salinity was markedly different than the other sites, suggesting yet another source of fDOM (Fig. 6). Significant wave height was less than 0.05 m, peaking during the frontal passage of 1 September 2013 (Fig. 3); peak wave height was 0.07 m. Wave period ranged from 1.0 to 4.0 s; peak wave periods over 6 s were observed regularly (not shown). At the channel site, wave heights were over 0.1 m (not shown). We discuss the diminished sediment resuspension response to wave forcing at sites LVL_{sh} and TS_{sh} in the following section.

3.2 Spatial variability of median measurements

The median values of physical forcings, light attenuation, and constituents demonstrate a large spatial gradient of external forcings and water quality in Barnegat Bay (Table 1). While tidal velocity was relatively similar over all shoal sites, median wave height was minimized at the northern site LVL_{sh}, where limited fetch likely contributes to reduced wave heights. The south-to-north salinity gradient is caused by substantially higher river outflow from northern tributaries such as the Toms and Metedeconk Rivers. This transport, coupled with higher nutrient loading in the north (Kennish et al., 2007) likely explains the increased chl-a and fDOM in the northern bay. However, light attenuation is maximized in the southern bay at site LEI_{sh} due to elevated turbidity. Both fDOM and chl-a were minimized at this site, due to reduced freshwater and nutrient loading. Measurements at the continuously occupied site Mantoloking indicate that the sequential nature of our deployments did not complicate interpretation of these patterns: turbidity was relatively constant throughout the summer, while neither fDOM nor chl-a increased as summer progressed, while there was an increase spatially as sites were occupied from south-to-north).

3.3 Sediment composition

Samples were collected at 9 locations near sites LVL_{sh} and TS_{sh}, and 12 locations southwest of LEI_{sh}, as well as one sample adjacent to each deployment site (Fig. 7). Grain-size analyses revealed a coarsening of sediment from south to north (Table 2). Samples collected adjacent to site LEI_{sh} had over double the clay percentage of the other sites and less sand. Median particle diameter D_{50} at site LEI_{sh} was in the medium silt range, while D_{50} was in the very fine sand and coarse silt range at sites TS_{sh} and LVL_{sh}, respectively. Sites TS_{sh} and LVL_{sh} both reside on the landward side of the barrier island, which has historically been subjected to overwash events (Donnelly et al., 2007). Overwash processes deposit sand on the landward side of the barrier island into the estuary leading to coarser deposits in these areas (Oertel, 1985). Conversely, site LEI_{sh} is on the landward side of the estuary adjacent to the mainland, which is fringed by extensive marsh. These marshes represent a local source of fine sediment that can be released during marsh collapse under wave forcing (Mariotti and Fagherazzi, 2013; Ganju et al., 2013).

4 Discussion

4.1 Relative contributions to light attenuation

The application of Eq. 2 allows for estimating the relative contributions of turbidity, chl-a, and CDOM to light attenuation at each site (Table 3). Turbidity dominated the light attenuation at site LEI_{sh}, while chl-a was dominant at site TS_{sh}; CDOM was important at site LVL_{sh} (though secondary to turbidity) due to its proximity to freshwater sources such as the Toms River. These results suggest that physical processes (sediment resuspension and advection) are dominant at sites LEI_{sh} and LVL_{sh}, while water-quality processes (nutrient loading and phytoplankton proliferation) are more important at site TS_{sh}. This is supported by the residence time calculations of Defne and Ganju (~~in revision~~2014) that demonstrate areas between sites TS_{sh} and LVL_{sh} are poorly flushed, leading to less dilution of estuarine waters by seawater and enhancing phytoplankton proliferation.

Before implementing the light model, we removed the effect of non-photochemical quenching (Fig. 4) by eliminating chl-a measurements during periods when PAR exceeded 50 $\mu E/m^2/s$ and filling the gaps using linear interpolation. We selected an initial slope of fDOM fluorescence to CDOM absorbance based on measurements from several estuaries (Chen et

al., 2008). We then applied the model with the default parameters noted above (Table 4), and compared modeled K_{dPAR} to the field measurements at each site. We modified three parameters selectively based on correlations between residual error and the different constituents to obtain the highest correlation and lowest error (Fig. 8). Attempts at a standard multiple linear regression model led to spurious results in some cases (e.g. inverse relationship between fDOM and K_{dPAR} at site LVL_{sh}). The variability in the fDOM vs. salinity relationship supports the possibility that the source and optical properties of colored organic matter varies spatially in Barnegat Bay~~.~~; Oestreich et al. (2014) demonstrated large spatial variability in CDOM absorbance potential per unit fluorescence, as a function of source. Spectral slope within Barnegat Bay varied by approximately 15%, resulting in calculated changes to K_{dPAR} of less than 4%. Additionally, variability in turbidity and organic content of suspended sediment also suggests that particulate backscatteringing ratio may be spatially variable; suspended-sediment samples demonstrated organic content ranging from 13% at site LEI to 60% at site LVL. The backscattering ratio change from 0.015 to 0.025 at LEI_{sh} is within the range (0.0024 to 0.06, Loisel et al., 2007 and Snyder et al., 2008) provided by Gallegos et al. (2011). While scattering by organic particles is strongly in the forward direction (smaller value of $b_{b(part)}$), mineral particles, having larger refraction indices, scatter a greater fraction of light in the backward direction (larger $b_{b(part)}$). The dependency of backscattering on particle size results in smaller modifications of $b_{b(part)}$ than the refraction index differences between organic and mineral particles (Gallegos et al., 2011). Thus a larger backscattering ratio was expected ~~given~~in the areas with higher turbidity~~.~~ (site LEI). Finally, marked variability in phytoplankton community composition suggests that chlorophyll absorbance at specific wavelengths may be variable (Ren, 2013). The chlorophyll-specific absorption coefficients of natural phytoplankton ($a_{\phi,675}$) exhibit substantial variability (Bricaud et al., 1995) with higher values for oligotrophic waters and smaller coefficients for eutrophic environments, which is consistent with the lower absorption coefficient chosen for LVL_{sh} (highest chl-a concentration).

At the lower end of the comparison between observed and modeled K_{dPAR} (i.e. modeled K_{dPAR} <1.6), we find reduced sensitivity of the model to changes in observed turbidity, chl-a, and fDOM. This could be due to changes in either particle characteristics or other effects that would be more obvious at low attenuation, such as interference from surface waves. It is also possible that the model parameterization for the three attenuating substances fails at the low end because the parameters (Table 4) are not static. We are also assuming that constituent

Formatted: Font: Not Italic

Formatted: Font: Not Italic

Formatted: Font: Not Italic

Formatted: Font: Not Italic

concentrations are uniform between the two PAR sensors; changes in vertical gradients between quiescent and energetic periods could also alter the agreement. We chose to optimize the relationship for high K_{dPAR}, but could have alternatively selected parameters to optimize for agreement at the low end.

Formatted: Font: Italic

Formatted: Font: Italic, Subscript

4.2 Temporal and spatial variability in light attenuation

Many prior studies and current estuarine monitoring protocols utilize infrequent (e.g. daily or weekly) sampling for water quality parameters including light attenuation (or secchi depth as a proxy). We found that temporal variability in light attenuation at each site was much larger than the difference between the median values at the three sites. At site LEI_{sh}, maximum K_{dPAR} was over 7 m^{-1} during a wind event, which caused increased turbidity; during quiescent periods K_{dPAR} decreased to 1.2 m^{-1}. At site TS_{sh}, a storm/runoff event raised K_{dPAR} to a peak value of 2.8 m^{-1}; the minimum value was 0.8 m^{-1}. Another wind event led to a peak K_{dPAR} of 2.9 m^{-1} at site LVL_{sh}, while the minimum value was under 1.0 m^{-1}. Daily or weekly sampling would not capture this variability and sampling during a peak or minimum event (more likely, as sampling is biased towards calm conditions) may skew the resulting interpretation of light penetration. We find that daily sampling at a set time (8:00 am local time, in this case) resulted in mean light attenuation errors ranging from 2% at site TS to 17% at site LEI. Sites with large temporal variability in constituents, like turbidity, will likely have the largest increases in error as sampling interval is lengthened. While it is cost-prohibitive to monitor light attenuation continuously at multiple sites, spatial and temporal patterns deduced from infrequent measurements should be interpreted with care or supplemented by more complete measurements (e.g. proxy measurements or modeling).

Spatially, the increased light attenuation in the south is mainly forced by turbidity. Regular resuspension and advection events on tidal and diurnal timescales (Figs. 2, 3, 6) increase turbidity and light attenuation at site LEI_{sh} throughout the deployment. Moving northward, light attenuation is governed increasingly by biogeochemical components, congruent with the longer residence time and decreased flushing in the northern bay (Defne and Ganju, ~~in revision~~2014). The northern bay is also subjected to elevated nutrient loads from the more developed watershed (Kennish et al., 2007). Conversely, the southern portion of the bay is fringed by wetlands, which represent a large source of fine sediment through shoreline erosion (see below). This pattern suggests a south-to-north gradient in light attenuation that is

forced by a south-to-north gradient in physical forcing, sediment availability, and nutrient loading.

4.3 Sediment transport on the shoals: resuspension mechanisms and fine sediment supply

Sediment sampling confirmed a greater abundance of clay-sized material in the southern bay, suggesting an increased likelihood of resuspension under wave forcing. We computed wave-current combined bed shear stresses (Madsen, 1994) at the three shoal sites and found varying resuspension responses to bed stress. At sites LEI_{sh} and TS_{sh}, turbidity responded linearly with stress; but turbidity was nearly 5 times larger at site LEI_{sh} for a given stress (Fig. 9). This confirms a larger repository of erodible material at the site, likely due to supply from adjacent wetlands. Samples closest to site TS_{sh} indicate that the bed is nearly all sand-sized material, which would only be resuspended at the highest stresses (Fig. 9). At site LVL_{sh}, the weak correlation and diminished resuspension response suggests a limited pool of erodible material. The secondary spectral density peak at the M_2 tidal period at LEI_{sh} (Fig. 4) raises the possibility that sediment advection from a far-field source may be important, and that local resuspension is not dominant. Waves accounted for 56% of the calculated shear stress at site LEI_{sh}, 64% at site TS_{sh}, and 45% at site LVL_{sh}.

Turbidity measurements at all channel/shoal-paired sites show that longitudinal (north-south) variability was larger than lateral (channel-shoal) variability (Table 5). Median and extreme (99%) values of turbidity were similar between paired sites; correlation was highest in the south (where forcing was consistent) and lower in the north where episodic events dominated. Estuarine shoals are typically subjected to greater wind-wave resuspension than channels, but the channels are the conduit for subsequent advection of suspended sediment. Given the dominance of shoals in Barnegat Bay, it is not surprising that channels adjacent to shoals are influenced by shoal processes. As discussed above however, the longitudinal variability in sediment source and availability explains the large longitudinal gradient in turbidity and light attenuation. From a sampling point-of-view, it appears that dense longitudinal sampling is more critical than lateral sampling, at least for turbidity and suspended-sediment concentration. The role of submerged aquatic vegetation in shoal resuspension processes can be substantial. Seagrass canopies can alter the velocity profile (Lacy and Wyllie-Echeverria, 2011) and dampen waves (Fonseca and Cahalan, 1992). While we did not quantify the effect

of seagrass meadows on these processes, it is possible that differences in vegetative density and areal coverage could modify the response of the seabed to a given resuspension event.

4.4 Role of vessel wakes in sediment resuspension

Due to the frequent resuspension and advection events at site LEI_{sh} (relative to the northern sites), we focused our analysis of vessel-induced sediment resuspension on this site. At the shoal site the ratio of 20 s significant wave height to 20 min significant wave height hovered about 1, indicating almost no local vessel wakes, while the ratio fluctuated widely at the channel site (Fig. 10). Turbidity between the channel and shoal was well-correlated with similar medians and extreme values (Table 5); however correlation between wave height and wind speed is weak at the channel site (r^2=0.03) but strong at the shoal site (r^2=0.44). Similarly, correlation between turbidity and wave height at the channel site is extremely low ($r^2 < 0.01$) while it is high at the shoal site (r^2=0.52). This suggests that local resuspension from wind-waves is responsible for increased turbidity at the shoal site, and that advection from shoals is responsible for increases in turbidity at the channel site. It also suggests that the shoal site is representative of a broader area; i.e. diurnal winds over the entire southern bay increase turbidity throughout the area allowing for advection into the channels. Wave heights in the channel tended to peak in the late afternoon (local time) though the peak of wake occurrence varied, while wave heights over the shoal peaked during the period of maximum winds. We also estimated wave heights over the shoals with a fetch-limited, shallow water approximation (USACE, 1984) and with a SWAN (Booij et al., 1999) wave model of Barnegat Bay forced with steady winds in the northerly direction. These simulations show that the observed winds are more than capable of causing the observed waves, without invoking vessel wakes (Fig. 11). However, given the separation between the sites it is likely that vessel wakes in the channel are attenuated rapidly as they encounter the channel-shoal transition. At these locations it is possible that turbidity is locally enhanced, but this is not reflected in either channel or shoal measurements.

4.5 Influence of regulation, ESA status, and vessel traffic on light attenuation

Increased population in the Barnegat Bay region has led to concerns about the effect of recreational boating on estuarine ecological function (EPA, 2007). In response to these concerns, Environmentally Sensitive Areas (ESAs) were established to ostensibly protect seagrass-colonized shoals from scarring and sediment resuspension due to vessel traffic

(NJDEP, 2012). We occupied three distinct vegetated shoal habitats in Barnegat Bay, each representing a different combination of protection and anthropogenic exposure (Lathrop and Haag, 2011): 1) a protected ESA near an area with lower coastal development and vessel harborage (site LEI_{sh}); 2) a protected ESA with relatively high recreational vessel traffic (site TS_{sh}); and 3) an unprotected site with relatively high recreational vessel traffic (ste LVL_{sh}). Our results show that physical variables (wind-wave resuspension, sediment availability) outweigh both protection and potential vessel traffic in terms of light attenuation over seagrass meadows. Site LEI_{sh} is designated for protection, yet light attenuation is maximized at that site due to wind-waves and sediment resuspension. Both of these parameters are outside the sphere of regulation and suggest that a future decrease in light attenuation to seagrass meadows at this site is unlikely (in lieu of a long-term depletion of sediment supply). It should be noted that protection does decrease the likelihood of propeller scarring, something this study does not address. The light attenuation and constituent measurements provide an estimate of what gains can be made through reduction of anthropogenic nutrient loads. Sites TS_{sh} and LVL_{sh} stand to benefit the most from mitigation of eutrophication as phytoplankton concentrations may decrease with nutrient loading reductions. This will also diminish the proliferation of macroalgae, which compete with seagrass and have been implicated in seagrass loss.

5 Conclusions

Understanding the temporal and spatial variability of light attenuation is critical for establishing potential success of seagrass community restoration and estimating the recovery of estuaries from eutrophication. We quantified light attenuation and dissolved and particulate light inhibitors with high-temporal resolution in three seagrass meadows of Barnegat Bay, New Jersey. We found a strong south-to-north gradient in light attenuation that is mainly forced by turbidity and sediment supply in the southern part of the bay. Regular wind-wave resuspension, infrequent storms, and runoff events all contributed to sizable temporal fluctuations in light attenuation at all shoal sites. Individual storms were capable of doubling light attenuation over periods longer than 1 d through wind-wave resuspension and increased river flow. Changing patterns of storm intensity and frequency may have a long-term effect on the light climate in back-barrier estuaries. Wave heights and turbidity over the shoals appeared to be the result of wind rather than vessel traffic. Light attenuation was lowest in the

most trafficked areas of the estuary, indicating that direct impact of vessel wakes on light attenuation is minimal. Spatial and temporal data of this type are necessary for modeling the response of seagrass communities to sea-level rise, storms, and nutrient loading. Numerical models of hydrodynamics, sediment transport, and ecology can be constrained with these measurements and used to guide restoration and habitat characterization.

Acknowledgements

Funding was provided by the New Jersey Department of Environmental Protection and the U.S. Geological Survey Coastal and Marine Geology Program. The authors thank the Rutgers University Marine Field Station for their support, especially Tom Malatesta, Roland Hagan, Rose Petrecca, and Ken Able. Field and analytical support was provided by Sandy Baldwin, Jon Borden, Zafer Defne, Patrick Dickhudt, and Kate McMullen. Charles Gallegos graciously provided light model code, and Emmanuel Boss offered helpful suggestions for data analysis. Jessie Lacy and John Pohlman provided helpful comments on the manuscript. Any use of trade, firm, or product names is for descriptive purposes only and does not imply endorsement by the U.S. Government.

Author Contributions

N.K.G. designed the time-series experiment and analyzed the time-series data, A.L.A. implemented the light model, and J.L.M. designed the sediment sampling program and analyzed the surficial sediment data. All authors contributed to the drafting of the manuscript.

References

Biber, P.D., Gallegos, C.L., Kenworthy, W.J.: Calibration of a bio-optical model in the North River, NC: A tool to evaluate water quality impact on seagrasses, Estuaries and Coasts, 31, 177-191, 2008.

Booij, N., Ris, R.C., Holthuijsen, L.H.: A third-generation wave model for coastal regions 1. Model description and validation, Journal of Geophysical Research 104, 7667–7681, 1999.

Boss, E., Twardowski, M.S., Herring, S.: Shape of the particulate beam attenuation spectrum and its inversion to obtain the shape of the particulate size distribution, Appl. Opt., 41, 4885-4893, 2001

Bowers, D. G. and Binding, C.E.: The optical properties of mineral suspended particles: A review and synthesis, Estuarine Coastal Shelf Sci., 67, 219–230, 2006.

Bricaud, A., Babin, M., Morel, A., and Claustre, H.: Variability in the chlorophyll-specific absorption coefficients of natural phytoplankton: Analysis and parameterization, J. Geophys. Res., 100, 13321–13332, 1995.

Bricaud, A., Morel, A., and Prieur, L.: Absorption by dissolved organic matter of the sea (yellow substance) in the UV and visible domains, Limnol. Oceanogr., 26, 43–53, 1981.

Brodtkorb, P.A., Johannesson, P., Lindgren, G., Rychlik, I., Ryden, J., Sjo, E.: WAFO—a Matlab toolbox for analysis of random waves and loads, Proceedings of the 10th International Offshore Polar Engineering Conference, Seattle, WA, III, p. 343–350, 2000.

Burkholder, J. M., Tomasko, D. A., and Touchette, B. W.: Seagrasses and eutrophication, Journal of Experimental Marine Biology and Ecology, 350, 46-72, 2007.

Chant, R. J.: Tidal and subtidal motion in a shallow bar-built multiple inlet/bay system, Journal of Coastal Research, SI32, 102-114, 2001.

Chen, R.F., Gardner, B., Huang, W., and Peri, F.: Chromophoric Dissolved Organic Matter (CDOM) in United States Estuaries, Proceedings of the 10th IEBS, Xiamen, China, May 18-22, 2008.

Christian, D. and Sheng, Y. P.: Relative influence of various water quality parameters on light attenuation in Indian River Lagoon, Estuarine, Coastal and Shelf Science, 57, 961-971, 2003.

Collias, E.E., Rona, M.R., McManus, D.A., and Creager, J.S.: Machine processing of geological data. University of Washington Technical Report, no. 87, 1963.

Defne, Z. and Ganju, N.K.: Quantifying the residence time and flushing characteristics of a shallow, back-barrier estuary: application of hydrodynamic and particle tracking models, Estuaries and Coasts, ~~in revision~~1-16, 2014.

Donnelly, J. P., Roll, S., Wengren, M., Butler, J., Lederer, R., and Webb, T.: Sedimentary evidence of intense hurricane strikes from New Jersey, Geology, 29, 615-618, 2001.

Downing, B. D., Boss, E., Bergamaschi, B. A., Fleck, J. A., Lionberger, M. A., Ganju, N. K., Schoellhamer, D.H., and Fujii, R.: Quantifying fluxes and characterizing compositional changes of dissolved organic matter in aquatic systems in situ using combined acoustic and optical measurements, Limnology and Oceanography: Methods, 7, 119-131, 2009.

Downing, B. D., Pellerin, B. A., Bergamaschi, B. A., Saraceno, J. F., and Kraus, T. E.: Seeing the light: The effects of particles, dissolved materials, and temperature on in situ measurements of DOM fluorescence in rivers and streams, Limnology and Oceanography: Methods, 7, 767-775, 2012.

Environmental Protection Agency: National Estuary Program Coastal Condition Report, Chapter 3: Northeast National Estuary Program Coastal Condition, Barnegat Bay National Estuary Program, http://www.epa.gov/owow/oceans/nepccr/index.html, 2007.

Folk, R.L.: Petrology of Sedimentary Rocks, Hemphill Publishing Co., Austin, Texas, 1974.

Gallegos, C.L., Werdell, P.J., and McClain, C.R.: Long-term changes in light scattering in Chesapeake Bay inferred from Secchi depth, light attenuation, and remote sensing measurements, J. Geophys. Res. 116, C00H08, doi:10.1029/2011JC007160, 2011.

Fonseca, M. S. and Cahalan, J. A.: A preliminary evaluation of wave attenuation by four species of seagrass, Estuarine, Coastal and Shelf Science, 35, 565-576, 1992.

Ganju, N. K., Nidzieko, N. J., and Kirwan, M. L.: Inferring tidal wetland stability from channel sediment fluxes: Observations and a conceptual model, Journal of Geophysical Research: Earth Surface, 118, 2045-2058, 2013.

Ganju, N. K., Schoellhamer, D. H., Warner, J. C., Barad, M. F., and Schladow, S. G.: Tidal oscillation of sediment between a river and a bay: a conceptual model, Estuarine, Coastal and Shelf Science, 60, 81-90, 2004.

Glibert, P. M., Wazniak, C. E., Hall, M. R., and Sturgis, B.: Seasonal and interannual trends in nitrogen and brown tide in Maryland's coastal bays, Ecological Applications, 17, 79-87, 2007.

Howarth, R. W. and Marino, R.: Nitrogen as the limiting nutrient for eutrophication in coastal marine ecosystems: evolving views over three decades, Limnology and Oceanography, 51, 364-376, 2006.

Kennish, M. J., Fertig, B. M., and Sakowicz, G. P.: In situ Surveys of Seagrass Habitat in the Northern Segment of the Barnegat Bay-Little Egg Harbor Estuary: Eutrophication Assessment, http://bbp.ocean.edu/Reports/2011%20Northern%20seagrass%20survey.pdf, 2013.

Kennish, M. J., Fertig, B.M., and Sakowicz, G. P.: Benthic macroalgal blooms as an indicator of system eutrophy in the Barnegat Bay–Little Egg Harbor estuary, Bulletin of the New Jersey Academy of Science, 56, 1-5, 2011.

Kennish, M.J., Bricker, S.B., Dennison, W.C., Glibert, P.M., Livingston, R.J., Moore, K.A., Noble, R.T., Paerl, H.W., Ramstack, J.M., Seitzinger, S., Tomasko, D.A., and Valiela, I.: Barnegat Bay–Little Egg Harbor Estuary: case study of a highly eutrophic coastal bay system, Ecological Applications 17, 3–16, 2007.

Kirk, J. T. O.: Light and photosynthesis in aquatic ecosystems, Cambridge University Press, 1994.

Lacy, J. R. and Wyllie-Echeverria, S.: The influence of current speed and vegetation density on flow structure in two macrotidal eelgrass canopies, Limnology and Oceanography: Fluids and Environments, 1, 38-55, 2011.

Lathrop, R.G. and Haag, S.M.: Assessment of seagrass status in the Barnegat Bay-Little Egg Harbor Estuary system: 2003 and 2009, Center for Remote Sensing and Spatial Analysis report, 2011.

Lathrop, R. G., Montesano, P., and Haag, S.: A multi-scale segmentation approach to mapping seagrass habitats using airborne digital camera imagery, Photogrammetric Engineering and Remote Sensing, 72, 665-675, 2006.

Lawrenz, E. and Richardson, T. L.: How does the species used for calibration affect chlorophyll a measurements by in situ fluorometry?, Estuaries and Coasts, 34, 872-883, 2011.

Lawson, S. E., Wiberg, P. L., McGlathery, K. J., and Fugate, D. C.: Wind-driven sediment suspension controls light availability in a shallow coastal lagoon, Estuaries and Coasts, 30, 102-112, 2007.

Lee, Z.-P., Du, K.-P., and Arnone, R.: A model for the diffuse attenuation coefficient of downwelling irradiance, J. Geophys. Res., 110, C02016, doi:10.1029/2004JC002275, 2005.

Loisel, H., Mériaux, X., Berthon, J.-F., and Poteau, A.: Investigation of the optical backscattering to scattering ratio of marine particles in relation to their biogeochemical composition in the eastern English Channel and southern North Sea, Limnol. Oceanogr., 52, 739–752, doi:10.4319/lo.2007.52.2.0739, 2007.

Madsen, O.S.: Spectral wave–current bottom boundary layer flows, Proceedings of the 24th International Conference Coastal Engineering Research Council, Kobe, Japan, 1994.

Mariotti, G. and Fagherazzi, S.: Critical width of tidal flats triggers marsh collapse in the absence of sea-level rise, Proceedings of the National Academy of Sciences, 110, 5353-5356, 2013.

Maxwell, K. and Johnson, G. N.: Chlorophyll fluorescence—a practical guide, Journal of Experimental Botany, 51, 659-668, 2000.

McGlathery, K. J., Anderson, I. C., and Tyler, A. C.: Magnitude and variability of benthic and pelagic metabolism in a temperate coastal lagoon, Marine Ecology Progress Series, 216, 1-15, 2001.

Meyercordt, J., Gerbersdorf, S., and Meyer-Reil, L. A.:. Significance of pelagic and benthic primary production in two shallow coastal lagoons of different degrees of eutrophication in the southern Baltic Sea, Aquatic Microbial Ecology, 20, 273-284, 1999.

Mobley, C. D. and Stramski, D.: Effects of microbial particles on oceanic optics: Methodology for radiative transfer modeling and example simulations, Limnol. Oceanogr., 42, 550–560, 1997.

New Jersey Department of Environmental Protection: Environmentally Sensitive Areas Guidance Document, http://www.nj.gov/dep/rpp/brp/dp/downloads/DPCC_ Environmentally_ Sensitive_Areas_Guidance.pdf, 2012.

Oertel, G. F.: The barrier island system, Marine Geology, 63, 1-18, 1985.

Oestreich, W. K., Ganju, N.K., Pohlman, J.W., and Suttles, S.E.: Colored dissolved organic matter in shallow estuaries: the effects of source and transport on light attenuation and measurement, American Geophysical Union Fall Meeting Abstracts, 2014.

Phlips, E. J., Badylak, S., and Grosskopf, T.: Factors affecting the abundance of phytoplankton in a restricted subtropical lagoon, the Indian River Lagoon, Florida, USA, Estuarine, Coastal and Shelf Science, 55, 385-402, 2002.

Phlips, E. J.: Chlorophyll a, tripton, color, and light availability in Florida Bay, USA, Marine Ecology Progress Series, 127, 223-234, 1995.

Poppe, L.J., Eliason, A.H., and Hastings, M.E.: A Visual Basic program to generate sediment grain-size statistics and to extrapolate particle distributions, Computers and Geosciences, 30, 791-795, 2004.

Preisendorfer, R. W.: Hydrologic Optics, 2, Foundations, Honolulu: US Dept. of Commerce, National Oceanic and Atmospheric Administration, Environmental Research Laboratories, Pacific Marine Environmental Laboratory, 1976.

Ren, L.: Baseline characterization of phytoplankton and harmful algal blooms in Barnegat Bay-Little Egg Harbor, New Jersey (year one), Final report to the New Jersey Department of Protection - Science and Research, 100 pp, 2013.

Schoellhamer, D. H.: Variability of suspended-sediment concentration at tidal to annual time scales in San Francisco Bay, USA, Continental Shelf Research, 22, 1857-1866, 2002.

Snyder, W. A., Arnone, R. A., Davis, C. O., Goode, W., Gould, R. W., Ladner, S., Lamela, G., Rhea, W. J., Stavn, R., Sydor, M. and Weidemann, A.: Optical scattering and backscattering by organic and inorganic particulates in U.S. coastal waters, Appl. Opt., 47, 666–677, doi:10.1364/AO.47.000666, 2008.

Spencer, R. G., Aiken, G. R., Dornblaser, M. M., Butler, K. D., Holmes, R. M., Fiske, G., Mann, P.J., and Stubbins, A.: Chromophoric dissolved organic matter export from US rivers. Geophysical Research Letters, 40, 1575-1579, 2013.

U.S. Army Corps of Engineers: Shore Protection Manual, v. 1 and 2, U.S. Army Corps of Engineers, Coastal Engineering Research Center, 1984.

Valentine, P. C., Blackwood, D. B., and Parolski, K. F.: Seabed Observation and Sampling System: US Geological Survey Fact Sheet FS-142-00, 2000.

Ziegler, S. and Benner, R.: Ecosystem metabolism in a subtropical seagrass-dominated lagoon, Marine Ecology Progress Series, 173, 1-12, 1998.

Table 1. RMS values of velocity (absolute value), and median values of wave height, salinity, light attenuation K_{dPAR}) and attenuating constituents from three sites and reference site Mantoloking. Value in parentheses at Mantoloking covers the same temporal overlap of the study sites.

	LEI_{sh}	TS_{sh}	LVL_{sh}	Mantoloking
RMS velocity (m/s)	0.06	0.05	0.07	N/A
Wave height (m)	0.02	0.02	0.01	N/A
Salinity (psu)	28	26	18	N/A
K_{dPAR} (m^{-1})	2.7 (1.9)[a]	1.4	1.4	N/A
Chl-a (RFU)[b]	12	21	24	9 (8, 4, 13)
fDOM (qsu)[c]	10	19	39	0.6 (1, 2, 0.2)
Turbidity (NTU)	12	6	6	6 (7, 7, 6)

[a]First value is from period with complete PAR data (26-30 June 2013), second value is reconstructed data for entire period (26 June – 16 July 2013) using Eq. 2

[b]Chl-a values at Mantoloking are reported in ug/L.

[c]fDOM values at Mantoloking are reported as CDOM in mg/L.

Table 2. Sediment grain-size results for combined samples collected near deployment sites with mini-SEABOSS grab sampler.

Parameter	LEI	TS	LVL
% sand	43	62	55
% silt	39	31	38
% clay	18	7	7
D_{50} (mm)	0.028	0.084	0.056

Table 3. Contributions to light attenuation from three constituents. The effect of water depth is removed from these calculations.

Constituent	LEI_{sh}	TS_{sh}	LVL_{sh}
Chl-a	17%	44%	22%
CDOM	14%	21%	36%
Turbidity	69%	35%	42%

Table 4. Parameters used for light model of Gallegos et al. (2011), Eq. 2: s_g = spectral slope of CDOM; $a_{\phi,675}$ = chlorophyll peak absorption; c_{x1} = baseline non-algal absorption; c_{x2} = non-algal absorption cross-section; s_x = non-algal spectral slope; $b_{b(water)}$ = backscattering by water molecules; $b_{b(part)}$ = backscattering by particulates.

Parameter	LEI_{sh}	TS_{sh}	LVL_{sh}
s_g (nm^{-1})[a]	0.0177	0.0177	0.0177
$a_{\phi,675}$ (m^2 mg^{-1})	0.0235	0.0235	0.0130
c_{x1} (m^2 g^{-1})[b]	0.0024	0.0024	0.0024
c_{x2} (m^2 g^{-1})[c]	0.04	0.04	0.04
s_x (nm^{-1})[d]	0.009	0.009	0.009
$b_{b(water)}$	0.5	0.5	0.5
$b_{b(part)}$	0.025	0.015	0.015

[a]Gallegos et al., 2011; [b]Biber et al., 2008; [c]Bowers and Binding, 2006; [d]Boss et al., 2001.

Table 5. Statistics and correlation of turbidity between channel and shoal at three sites.

Statistic	LEI_{sh}	LEI_{chan}	TS_{sh}	TS_{chan}	LVL_{sh}	LVL_{chan}
r^2	0.38	--	0.30	--	0.24	--
50% (NTU)	12	13	5.7	6.0	6.2	6.9
99% (NTU)	54	47	14	22	18	14

Figure 1. Map of Barnegat Bay, on the New Jersey Atlantic coast. Shoal sites are marked with a star; channel sites are marked with a circle. Estuarine bathymetry is from recent USGS mapping (unpublished).

Figure 2. Time-series of water level, photosynthetically active radiation (PAR), light attenuation over the PAR spectrum (K_{dPAR}), turbidity, chlorophyll-a fluorescence (Chl-a), and fluorescing dissolved organic matter (fDOM) for each site, starting from the south on the left. Grey trace in bottom three panels are reference values from site Mantoloking.

Figure 3. Time-series of north-south winds (positive winds from the south), water level, significant wave height at shoal sites, and turbidity for each site, starting from the south on the left.

Figure 4. Spectral density of turbidity, chlorophyll-a, and fDOM time-series from three shoal sites. Dashed lines correspond to M_2 tidal period (0.5175 days) and the diurnal period (1 d). Note the difference in y-axis scaling at LEI_{sh} in comparison to the other two sites.

Figure 5. Relationship between binned near-surface irradiance in the PAR spectrum (400-700 nm) and measured chlorophyll-a fluorescence. Bounds are one standard deviation of measured fluorescence within each bin. Fluorescence decreases with irradiance at all shoal sites, indicating substantial non-photochemical quenching (NPQ) of fluorescence.

Figure 6. Relationship between salinity and fDOM at three shoal sites, with linear regressions for each population. The three sites appear distinct, suggesting variability in the nature of the fDOM source.

Figure 7. Surficial sediment composition adjacent to deployment sites. A higher abundance of clay sized sediment is available near site LEI as compared to the other sites.

Figure 8. Agreement between observed K_{dPAR} over the PAR spectrum and the spectral attenuation model of Gallegos (2011).

Figure 9. Relationship between wave-current combined shear stress and turbidity at three shoal sites; darker symbols are instantaneous data binned and averaged in 0.01 Pa intervals. Site LEI_{sh} demonstrates enhanced resuspension as compared to other sites under similar stress conditions; surficial sediment distribution indicates a higher abundance of fine material in the southern part of the system.

Figure 10. Example of a single day of significant wave height (H_{sig}) data from sites LEI_{chan} and LEI_{sh}, and the ratio of 20-s window significant wave height (H_{sig20}) to 1200-s window significant wave height ($H_{sig1200)}$. The latter metric is used to identify vessel wakes, which are observed frequently at site LEI_{chan}, but seldom at site LEI_{sh}.

Figure 11. Measured and modeled wave-height response to wind at site LEI_{sh}; the USACE formulation neglects spatial variation in bathymetry, the SWAN model does not include the influence of tidal currents and assumes a constant, uniform wind field.